Editor's Choice MICROSCOPY

Microscopy, 2016, 370–377
doi: 10.1093/jmicro/dfw017
Advance Access Publication Date: 28 April 2016

Article

Direct observation of the actin filament by tip-scan atomic force microscopy

Akihiro Narita[1,2,*], Eiji Usukura[1], Akira Yagi[3], Kiyohiko Tateyama[3], Shogo Akizuki[1], Mahito Kikumoto[1], Tomoharu Matsumoto[1], Yuichiro Maéda[1], Shuichi Ito[3], and Jiro Usukura[1]

[1]Structural Biology Research Center, Graduate School of Science, Nagoya University, Nagoya 464-8602, Japan, [2]JST PRESTO, 4-1-8 Honcho, Kawaguchi, Saitama, 332-0012, Japan, and [3]R&D Group, Olympus Corporation, 2-3 Kuboyama-cho, Hachioji, Tokyo 192-8512, Japan

*To whom correspondence should be addressed. E-mail: narita.akihiro@f.mbox.nagoya-u.ac.jp

Received 23 December 2015; Accepted 28 April 2016

Abstract

Actin filaments, the actin–myosin complex and the actin–tropomyosin complex were observed by a tip-scan atomic force microscope (AFM), which was recently developed by Olympus as the AFM part of a correlative microscope. This newly developed AFM uses cantilevers of similar size as stage-scan AFMs to improve substantially the spatial and temporal resolution. Such an approach has previously never been possible by a tip-scan system, in which a cantilever moves in the *x*, *y* and *z* directions. We evaluated the performance of this developed tip-scan AFM by observing the molecular structure of actin filaments and the actin–tropomyosin complex. In the image of the actin filament, the molecular interval of the actin subunits (~5.5 nm) was clearly observed as stripes. From the shape of the stripes, the polarity of the actin filament was directly determined and the results were consistent with the polarity determined by myosin binding. In the image of the actin–tropomyosin complex, each tropomyosin molecule (~2 nm in diameter) on the actin filament was directly observed without averaging images of different molecules. Each tropomyosin molecule on the actin filament has never been directly observed by AFM or electron microscopy. Thus, our developed tip-scan AFM offers significant potential in observing purified proteins and cellular structures at nanometer resolution. Current results represent an important step in the development of a new correlative microscope to observe nm-order structures at an acceptable frame rate (~10 s/frame) by AFM at the position indicated by the fluorescent dye observed under a light microscope.

Key words: atomic force microscopy, tip-scan AFM, correlative microscopy, actin filament, tropomyosin, cytoskeleton

Introduction

Atomic force microscopy (AFM) has become an indispensable tool in the field of biology following its invention by Binning *et al.* [1] and subsequent further development [2]. The most outstanding recent development was high-speed AFM (HS-AFM) developed by Ando *et al.*, which can visualize movement and structural changes of proteins and other molecules in real time (recently reviewed in [3–6]). This type of HS-AFM is based on a sample-scan system. The stage can move the sample in the z-direction for maintaining a constant force and in the x–y directions for scanning the sample. HS-AFM does not require changing the x–y position of the cantilever and is relatively easy to control and detect the cantilever oscillation to sense the surface of the sample, which is one of the reasons they succeeded in inventing HS-AFM.

Although AFMs based on a sample-scan system has been used for observing proteins on plasma membranes [7], the application of this type of AFM has been limited to pure samples *in vitro*, whereas cellular structures are not suitable targets. The stage-scan HS-AFM cannot mount a large sample because the stage moves very fast for high-speed imaging. For example, a standard glass slide or cover slip is not available, which makes it difficult to mount the cell on the AFM stage. In addition, it is necessary to find the position of the cell on the stage with a light microscope because the scanning area of HS-AFM is severely limited. Unfortunately, this type of HS-AFM is also difficult to combine with light microscopy because of the difficulty in integrating a stage that moves fast.

In contrast, AFM based on a tip-scan system, in which the cantilever moves in the x, y and z directions and the stage does not move, has been applied to observe cellular structures [8–11] because it can be easily combined with any type of inverted light microscope without strict limitations on the sample size. Because the deflection of the small cantilever scanning in the x and y directions is difficult to sense, it had been challenging to apply a small cantilever, thereby limiting the time and spatial resolution of tip-scan AFM. A small cantilever is essential when scanning a specimen rapidly at a high spatial resolution. Olympus has developed a regulation system to control the cantilever and has thus been able to largely reduce the size of the cantilever. As a result, time resolution has been improved [12] and cell movement has been visualized by a newly developed tip-scan AFM combined with a fluorescent light microscope. Olympus has been developing a new AFM system named BIXAM [13], which is based on this technology and uses a similar size cantilever as the sample-scan HS-AFM system, and improves the time and spatial resolution dramatically. In this report, we observe directly the actin filament, the actin–myosin complex and the actin–tropomyosin complex by the AFM part of BIXAM to evaluate the performance in observing molecular structures. Actin filament polarity could be directly determined from AFM images, and each tropomyosin molecule on the actin filament was directly observed. Thus, our new tip-scan AFM offers significant potential for observing purified proteins and cellular structures at the molecular level.

Methods

Proteins

Actin, tropomyosin and myosin sub-fragment 1 (myosin S1) were purified from rabbit skeletal muscle, as described previously [14–16].

Specimen preparation for AFM observation

Actin filament and actin–myosin

Actin (0.1 mg ml^{-1}) was incubated for 30 min at room temperature in buffer A [50 mM NaCl, 10 mM sodium phosphate buffer (pH 7.4), 1 mM $MgCl_2$, 0.1 mM ATP and 1 mM dithiothreitol (DTT)]. Glass slides with 15 mm φ hydrophilic circular windows surrounded by the framework printed with hydrophobic black ink (TF0215; Matsunami Glass Ind., Ltd., Osaka, Japan) were used. To increase affinity toward the actin filament, the glass slide was coated with poly-lysine as follows: the glass slide was washed with ethanol twice, then washed with pure water twice and a poly-lysine solution (MW = 30,000–50,000; Sigma-Aldrich, St. Louis, MO, USA, 0.4 mg ml^{-1} dissolved in water) was applied and the slide washed three times with buffer A. Polymerized actin was diluted 10-fold with buffer A containing 1 µM phalloidin and applied to the poly-lysine-coated glass slide. The sample on the glass slide was then washed twice using buffer A containing 1 µM phalloidin.

For actin–myosin, actin (0.1 mg ml^{-1}) was incubated in buffer B [50 mM NaCl, 10 mM imidazole–HCl buffer (pH 7.4), 1 mM $MgCl_2$ and 1 mM DTT] for 30 min at room temperature, diluted 10-fold with buffer B containing 1 µM phalloidin and mounted onto the poly-lysine-coated glass slide. Myosin S1 was added (final 0.01 mg ml^{-1}) to the actin solution on the glass slide and incubated for >1 h to form the rigor complex at room temperature. The sample on the glass slide was washed twice with buffer B containing 1 µM phalloidin and then fixed in buffer B containing 0.5% glutaraldehyde and 1 µM phalloidin.

Actin–tropomyosin

Actin (0.24 mg ml^{-1}) and tropomyosin (0.24 mg ml^{-1}) were mixed and incubated for 30 min at room temperature in

buffer A. The solution was diluted 5-fold with buffer A containing 1 μM phalloidin and 0.5% glutaraldehyde. A small piece of newly cleaved mica was placed in the center of the window on the glass slide (TF0215). The sample solution was mounted onto the window on the glass slide with mica, washed twice with buffer A containing 1 μM phalloidin, and then glutaraldehyde was added to the solution (final concentration = 0.5%).

AFM measurement

The glass slide with the sample was mounted in BIXAM, a tip-scan type HS-AFM combined with an inverted fluorescent microscope (IX73; Olympus Corporation, Tokyo). For measurements at molecular resolution, AFM was set to the phase modulation mode [12] and small soft cantilevers with a spring constant of 0.1 N m^{-1} were used (BL-AC10DS, BL-AC10EGS; Olympus Corporation). The diameter of the scanning tip was ~8–10 nm. Images were collected with the speed set to one frame per 10 s.

Image analysis

To improve the signal-to-noise ratio of the AFM images, more than two sequential frames were taken and averaged for one region of interest. Drifting and rotation were considered in the averaging. Some images were multiplied by a filter in Fourier space (Fig. 1c) to achieve detailed information from the images by enhancing the high-resolution signal.

Simulation

The actin filament model [17] was placed along the *y*-axis in the computer. A sphere (a model for the AFM needle tip) with various diameters was generated at (x, y, z) coordinates. The initial z was larger than the maximum z position in the actin filament model + diameter. Then, the z was decreased until the sphere touched the actin filament model and the final z was plotted as a pixel value at (x, y) in the simulated image. When 1 nm^3 of the sphere overlapped with the actin filament model, we considered the sphere to be touching the actin filament.

Results

A typical AFM image of the actin filaments on the poly-lysine coated glass slide is presented in Fig. 1. Actin forms a double-stranded helical filament with a helix pitch of 36–38 nm along the strand, and the actin molecules are arranged with intervals of 5.5 nm in the strand [17–19]. The signal-to-noise ratio was improved (Fig. 1a and b) by averaging sequential frames, and the signal of the structure inside the filaments was enhanced (Fig. 1d) by multiplying the data with the filter (Fig. 1c). Clear stripes with intervals of 5.5 nm were observed

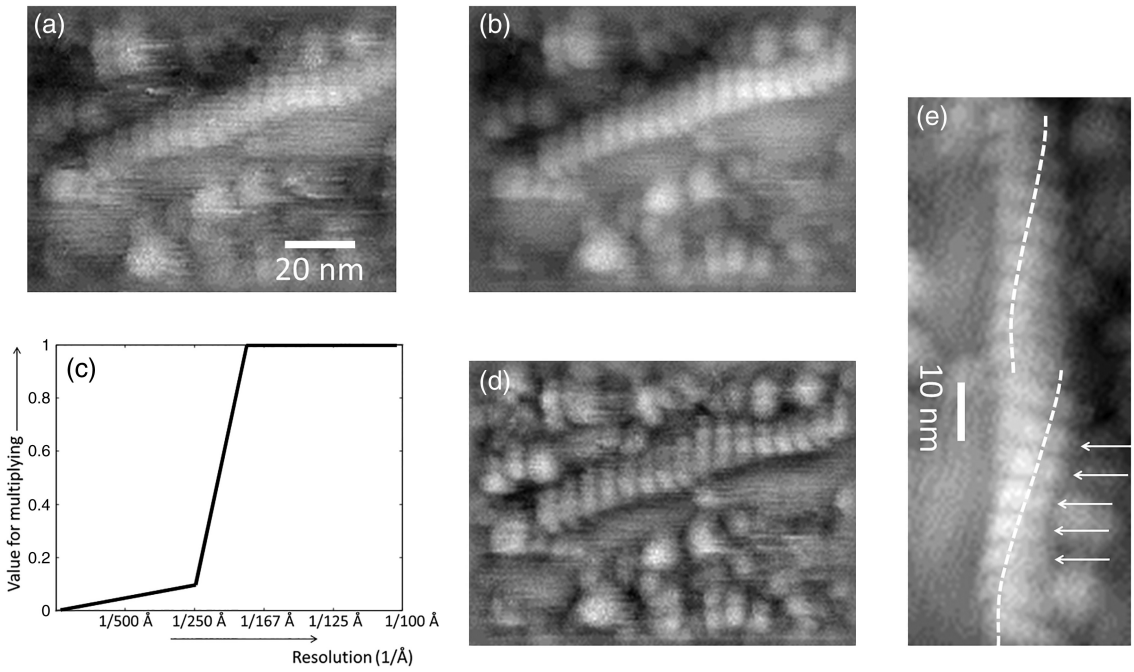

Fig. 1. Typical AFM image of the actin filament. (a) One typical AFM image of the actin filament before averaging. (b) Six frames were averaged. The signal-to-noise ratio was much improved. (c) Filter to enhance the high-resolution signal. (d) b multiplied by c in the reciprocal space. Details in the actin filament were enhanced. (e) Enlarged view of the actin filament (b). The long pitch helix along the strand is indicated by the white dotted lines, and the molecular interval along the strand is indicated by the white arrows.

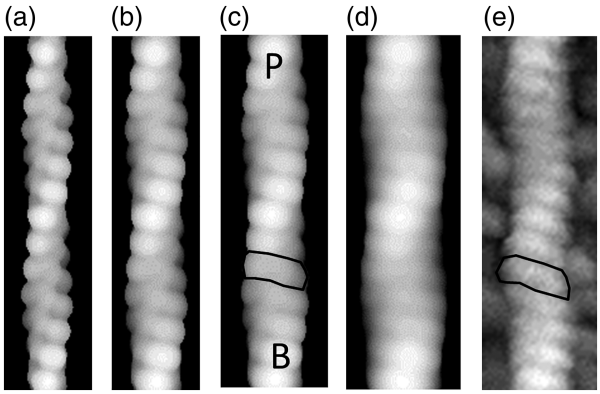

Fig. 2. (a–d) Simulated AFM images of the actin filament with 4, 6, 8 and 10 nm diameter spheres are presented in (a), (b), (c) and (d), respectively. The letters 'B' and 'P' in (c) represent the barbed end side and the pointed end side, respectively. (e) One AFM real image of the actin filament. A similar shape of stripes was observed in (c). One unit between stripes is enclosed by a black line in (c) and (e).

in all filaments, as well as the long pitch helix pattern of the actin filaments (Fig. 1e). The interval of the stripes corresponded to the actin molecular interval in the strand. To assess details of the images, we simulated the AFM image of the actin filament (Fig. 2). The simulation with an 8 nm diameter sphere, a model for the AFM needle tip, was very similar to the real image. Both the real images and the simulated image showed similar curvature in the stripes. The actin filament has polarity, and the two ends—barbed end and pointed end—have different properties in terms of polymerization and depolymerization rates [20,21]. In addition, most myosins move toward the barbed end. Thus, polarity determination is often essential for studying the properties of the actin filament *in vivo* [22] and *in vitro* [23,24]. The shape of the stripes reflects the polarity of the actin filament, and the concaved shape face corresponds to the barbed end of the actin filament (Figs 2 and 3). The polarity determined by the

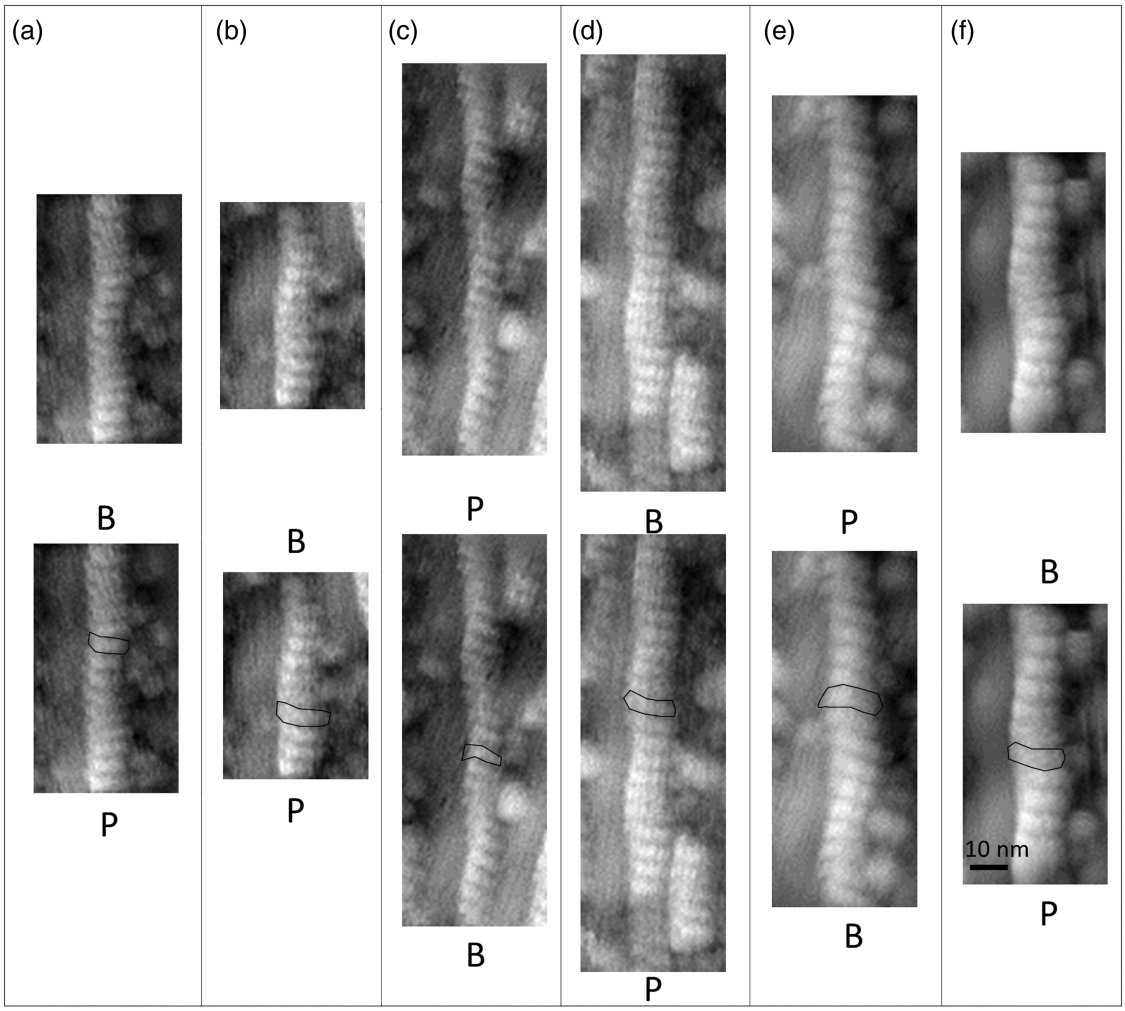

Fig. 3. (a–f) Gallery of actin filament images. Upper images: Original images. Lower images: One unit between stripes in each image is enclosed by a black line. The polarity of the filament was determined according to the shape of the stripes and indicated by the letters 'B' and 'P', the barbed end side and the pointed end side, respectively. Two, two, three, three, six and six frames were averaged for (a), (b), (c), (d), (e) and (f), respectively.

concaved shape was consistent with the polarity determined by myosin rigor binding [25,26]. Fifteen myosin heads bound to the actin filament with a similar tilt angle were observed, and all of them tilted toward the barbed end (Fig. 4). These results confirmed the determination of the polarity by the concaved shape of the stripes.

Actin–tropomyosin was also observed. Tropomyosin (~34 kDa) forms a dimeric coiled-coil spanning the entire length of a rod ~40 nm long, and the rod binds to the actin filament along the long pitch helix [27]. In the image of the actin–tropomyosin complex (Fig. 5), an extra elongated mass was clearly observed, which was absent in the images of the actin filament (Figs 1 and 3). It follows the long pitch helix of the actin filament, and the stripes of the actin filament could not be observed on the elongated mass. This is obviously tropomyosin, which was already visualized by single particle analysis or helical reconstruction [28,29], but this is the first time each tropomyosin on the actin filament has been clearly observed without averaging images of different molecules.

Discussion

We could clearly observe stripes of the interval of the actin subunits along the strand (~5.5 nm) and tropomyosin (~2 nm in diameter [30]) on the actin filament. These observations prove that BIXAM, a newly developed tip-scan AFM combined with a fluorescence microscope, has sufficient spatial resolution for nanometer order molecular structural observations. The time resolution of the tip-scan AFM, ~10 s/1 frame, is also acceptable although it is much slower than HS-AFM (~80 ms/1 frame). There is a report observing the actin filament structure by a tip-scan AFM [31] at similar resolution. However, it took several minutes

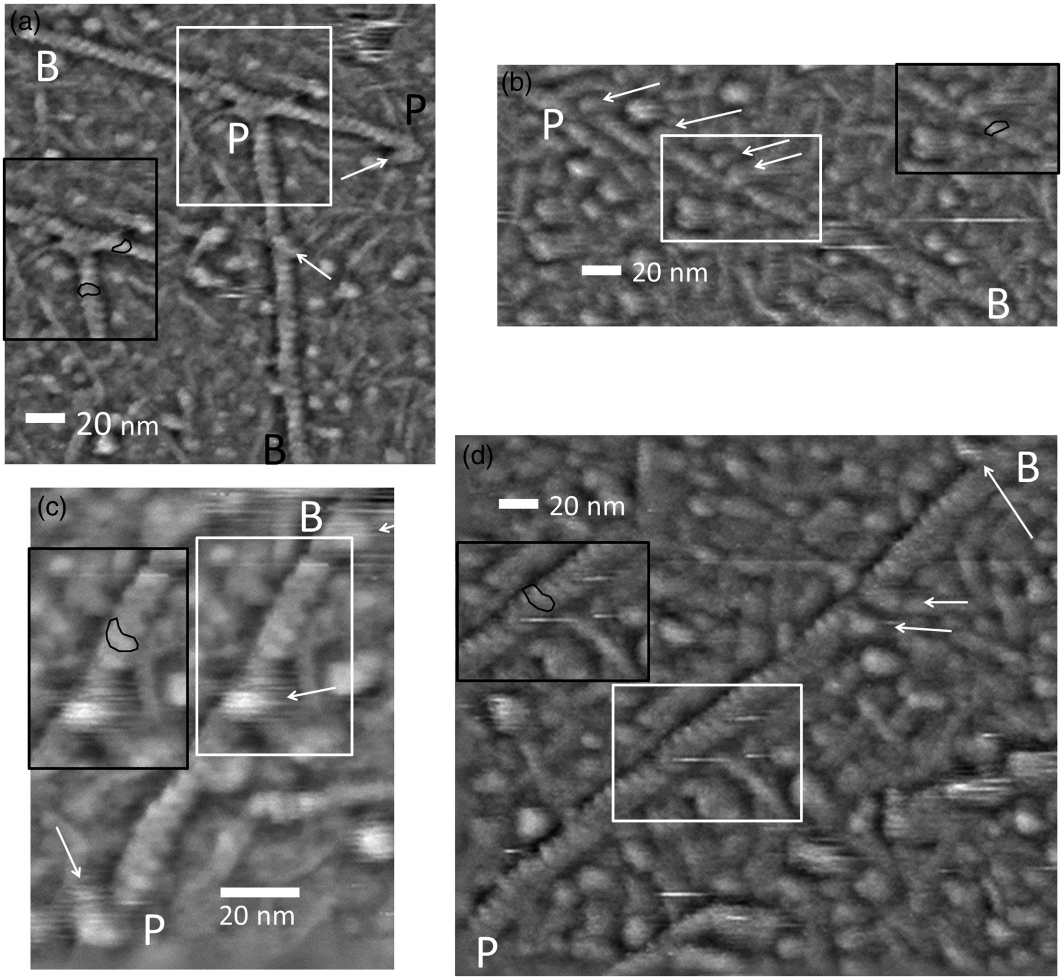

Fig. 4. (a–d) Actin–myosin S1 complexes. Myosin S1 binding is indicated by the white arrows. Insets enclosed by black lines represent the same position enclosed by white lines. In insets, one unit between stripes in each image is enclosed by a black line. The polarity was determined by the shape of the stripes and is indicated by the white letters 'B' and 'P'. All myosin S1 molecules were tilted toward 'B'; the determined barbed end side by the shape of the stripe. Four, four, nine and five image frames were averaged for (a), (b), (c) and (d), respectively. The averaged images were multiplied by the filter (Fig. 1c) in reciprocal space.

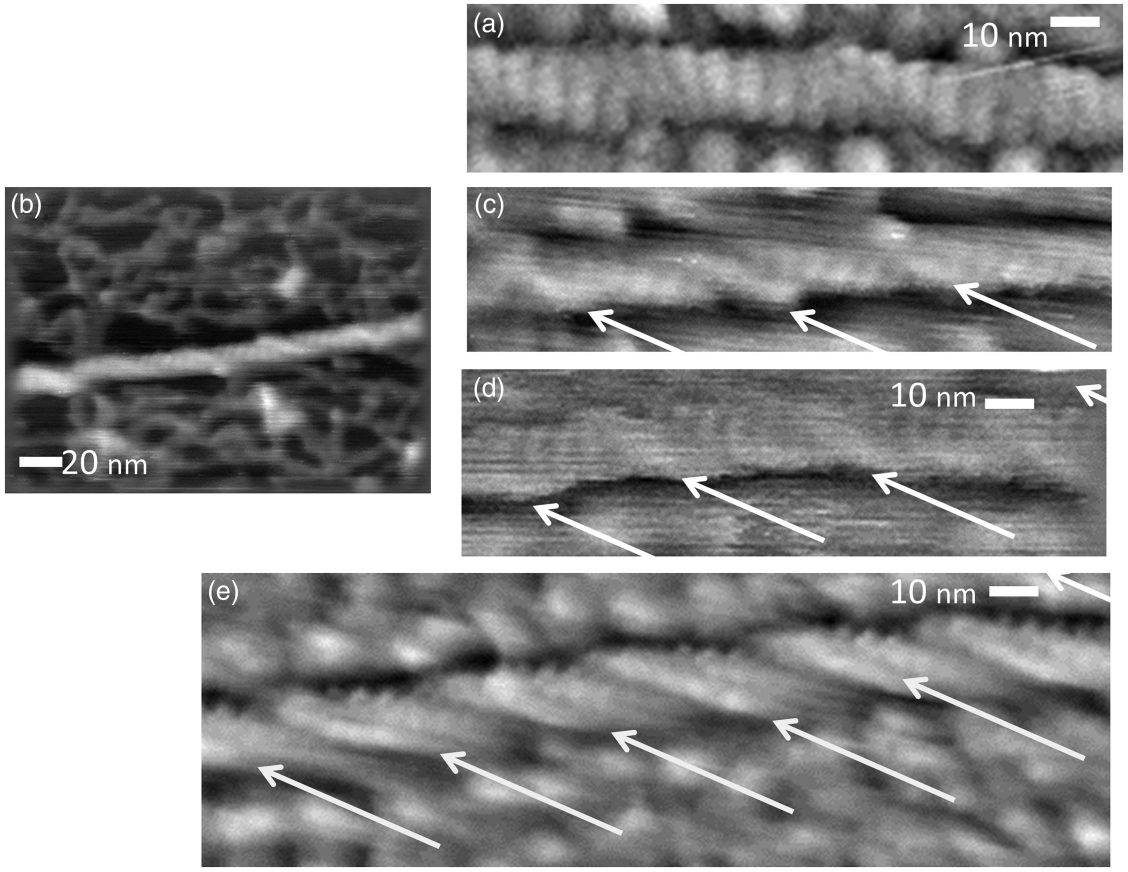

Fig. 5. Actin–tropomyosin complexes. (a) An AFM image of the actin filament without tropomyosin as a control. Nine frames were averaged. (b) One example of the actin–tropomyosin images. Seven frames were averaged. (c–e) Gallery of enlarged and high-resolution emphasized images of actin–tropomyosin. The elongated mass due to tropomyosin molecules are indicated by the white arrows. Seven, three and seven frames were averaged for (c), (d) and (e), respectively.

for one image because the resonant frequency of their cantilever was 7 kHz in solution and is therefore significantly slower than the BIXAM instrument presented herein (400 kHz in solution) [12].

Although X-ray crystallography, high-resolution single particle analysis and NMR have solved a large number of biomolecular structures, it is essential to understand how such biomolecules are integrated in cellular structures for linking high-resolution atomic structures to cellular functions. Electron tomography [22,32–34] and freeze-etching electron microscopy [35,36] have revealed molecular structures and arrangements in the cell to some extent. However, only the shape of the molecule can be observed in tomograms or EM images, and identification of molecules in complex cellular structures from EM images is often difficult. On the other hand, fluorescent labeling has rapidly developed, and this approach is suitable for relatively easy identification of molecules in the cell. Many cellular functions and phenomena have been observed by fluorescent microscopy, and it would be highly desirable to observe molecular structures at the position where a particular phenomenon is measured by fluorescent microscopy. Correlative microscopy [37–39] involves observing the position of the specimen by a light microscope and an electron microscope and is a good candidate to satisfy this purpose, linking atomic structures to cellular functions. However, sample preparation and observations are time-consuming and difficult because sample preparation for electron microscopy and light microscopy is completely different.

AFM based on a tip-scan system is another good candidate for correlative microscopy where molecular arrangements and aggregates can be observed directly. Specimen preparation is much easier than electron microscopy because the specimen can be observed in solution, and all of the fluorescent dyes for light microscopy can be used. Our tip-scan AFM represents satisfactory spatial resolution and frame rate and is also suitable for practical correlative microscopy.

However, the current light microscope in BIXAM does not have satisfactory sensitivity and resolution. Coupling with a light microscope is not trivial although it is much easier than using stage-scan AFM. Oil immersion, which is

required for high-resolution light microscopy, needs thin glass to mount specimens. This thin glass tends to vibrate owing to the AFM needle oscillation and limits AFM resolution. How to overcome the use of thin glass on the stage is the next most important step in realizing a practical correlative microscope.

Concluding remarks

A recently developed tip-scan AFM was able to visualize the actin molecular interval (5.5 nm) and tropomyosin on the actin filament (about 2 nm in diameter) at a much faster frame rate than previous tip-scan AFMs (10 s/frame). Our tip-scan AFM represents satisfactory spatial resolution and frame rate and is suitable for practical correlative microscopy, in which we can observe molecular structures and arrangements in the cell that are located near the fluorescent dye and that have been visualized by a light microscope. In principle, this AFM can be combined with any type of inverted light microscope and the coupling of this AFM system with a high-resolution light microscope is a future goal.

Funding

This research was supported by a Grant-in-Aid for Scientific Research (A) (JSPS KAKENHI Grant Number 26251017) from Japan Society for the Promotion of Science (to Y.M.). This research was also supported by PRESTO from the Japan Science and Technology Agency (to A.N.) and a collaboration research fund from Olympus Corp. (to A.N.). Funding to pay the Open Access publication charges for the article was provided by JST PRESTO.

References

1. Binnig G, Quate C F, Gerber C (1986) Atomic force microscope. *Phys. Rev. Lett.* 56: 930–933.
2. Engel A, Lyubchenko Y, Muller D (1999) Atomic force microscopy: a powerful tool to observe biomolecules at work. *Trends Cell Biol.* 9: 77–80.
3. Ando T (2014) High-speed AFM imaging. *Curr. Opin Struct. Biol.* 28: 63–68.
4. Ando T, Uchihashi T, Scheuring S (2014) Filming biomolecular processes by high-speed atomic force microscopy. *Chem. Rev.* 114: 3120–3188.
5. Uchihashi T, Watanabe H, Fukuda S, Shibata M, Ando T (2015) Functional extension of high-speed AFM for wider biological applications. *Ultramicroscopy* 160: 182–196.
6. Henderson R M (2015) Structural dynamics of single molecules studied with high-speed atomic force microscopy. *Expert Opin. Drug Discov.* 10: 221–229.
7. Muller D J, Hand G M, Engel A, Sosinsky G E (2002) Conformational changes in surface structures of isolated connexin 26 gap junctions. *EMBO J.* 21: 3598–3607.
8. Chacko J V, Zanacchi F C, Diaspro A (2013) Probing cytoskeletal structures by coupling optical superresolution and AFM techniques for a correlative approach. *Cytoskeleton (Hoboken)* 70: 729–740.
9. Trache A, Lim S M (2010) Live cell response to mechanical stimulation studied by integrated optical and atomic force microscopy. *J. Vis. Exp.* doi: 10.3791/2072.
10. Doak S H, Rogers D, Jones B, Francis L, Conlan R S, Wright C (2008) High-resolution imaging using a novel atomic force microscope and confocal laser scanning microscope hybrid instrument: essential sample preparation aspects. *Histochem. Cell Biol.* 130: 909–916.
11. Usukura J, Yoshimura A, Minakata S, Youn D, Ahn J, Cho S J (2012) Use of the unroofing technique for atomic force microscopic imaging of the intra-cellular cytoskeleton under aqueous conditions. *J. Electron Microsc.* 61: 321–326.
12. Suzuki Y, Sakai N, Yoshida A, Uekusa Y, Yagi A, Imaoka Y, Ito S, Karaki K, Takeyasu K (2013) High-speed atomic force microscopy combined with inverted optical microscopy for studying cellular events. *Sci. Rep.* 3: 2131.
13. Yoshida A, Sakai N, Uekusa Y, Deguchi K, Gilmore J L, Kumeta M, Ito S, Takeyasu K (2015) Probing in vivo dynamics of mitochondria and cortical actin networks using high-speed atomic force/fluorescence microscopy. *Genes Cells* 20: 85–94.
14. Spudich J A, Watt S (1971) The regulation of rabbit skeletal muscle contraction. I. Biochemical studies of the interaction of the tropomyosin–troponin complex with actin and the proteolytic fragments of myosin. *J. Biol. Chem.* 246: 4866–4871.
15. Okamoto Y, Sekine T (1985) A streamlined method of subfragment one preparation from myosin. *J. Biochem.* 98: 1143–1145.
16. Miki M (1987) The recovery of the polymerizability of Lys-61-labelled actin by the addition of phalloidin. Fluorescence polarization and resonance-energy-transfer measurements. *Eur. J. Biochem.* 164: 229–235.
17. Oda T, Iwasa M, Aihara T, Maeda Y, Narita A (2009) The nature of the globular- to fibrous-actin transition. *Nature* 457: 441–445.
18. Hanson J, Lowy J (1963) The structure of F-actin and of actin filaments isolated from muscle. *J. Mol. Biol.* 6: 46–60.
19. Holmes K C, Popp D, Gebhard W, Kabsch W (1990) Atomic model of the actin filament. *Nature* 347: 44–49.
20. Fujiwara I, Vavylonis D, Pollard T D (2007) Polymerization kinetics of ADP- and ADP-Pi-actin determined by fluorescence microscopy. *Proc. Natl Acad. Sci. U. S. A.* 104: 8827–8832.
21. Narita A, Oda T, Maeda Y (2011) Structural basis for the slow dynamics of the actin filament pointed end. *EMBO J.* 30: 1230–1237.
22. Narita A, Mueller J, Urban E, Vinzenz M, Small J V, Maeda Y (2012) Direct determination of actin polarity in the cell. *J. Mol. Biol.* 419: 359–368.
23. Ito T, Narita A, Hirayama T, Taki M, Iyoshi S, Yamamoto Y, Maeda Y, Oda T (2011) Human spire interacts with the barbed end of the actin filament. *J. Mol. Biol.* 408: 18–25.
24. Ito T, Hirayama T, Taki M, Iyoshi S, Dai S, Takeda S, Kimura-Sakiyama C, Oda T, Yamamoto Y, Maeda Y, Narita A (2011) Electron microscopic visualization of the filament binding mode of actin-binding proteins. *J. Mol. Biol.* 408: 26–39.

25. Rayment I, Holden H M, Whittaker M, Yohn C B, Lorenz M, Holmes K C, Milligan R A (1993) Structure of the actin–myosin complex and its implications for muscle contraction. *Science* 261: 58–65.
26. Behrmann E, Muller M, Penczek P A, Mannherz H G, Manstein D J, Raunser S (2012) Structure of the rigor actin–tropomyosin–myosin complex. *Cell* 150: 327–338.
27. Ebashi S, Endo M, Otsuki I (1969) Control of muscle contraction. *Q Rev. Biophys.* 2: 351–384.
28. Lehman W, Hatch V, Korman V, Rosol M, Thomas L, Maytum R, Geeves M A, Van Eyk J E, Tobacman L S, Craig R (2000) Tropomyosin and actin isoforms modulate the localization of tropomyosin strands on actin filaments. *J. Mol. Biol.* 302: 593–606.
29. Von Der Ecken J, Muller M, Lehman W, Manstein D J, Penczek P A, Raunser S (2015) Structure of the F-actin–tropomyosin complex. *Nature* 519: 114–117.
30. Phillips G N Jr, Fillers J P, Cohen C (1986) Tropomyosin crystal structure and muscle regulation. *J. Mol. Biol.* 192: 111–131.
31. Schmitz S, Schaap I A, Kleinjung J, Harder S, Grainger M, Calder L, Rosenthal P B, Holder A A, Veigel C (2010) Malaria parasite actin polymerization and filament structure. *J. Biol. Chem.* 285: 36577–36585.
32. Vinzenz M, Nemethova M, Schur F, Mueller J, Narita A, Urban E, Winkler C, Schmeiser C, Koestler S A, Rottner K, Resch G P, Maeda Y, Small J V (2012) Actin branching in the initiation and maintenance of lamellipodia. *J. Cell Sci.* 125: 2775–2785.
33. Medalia O, Weber I, Frangakis A S, Nicastro D, Gerisch G, Baumeister W (2002) Macromolecular architecture in eukaryotic cells visualized by cryoelectron tomography. *Science* 298: 1209–1213.
34. Nicastro D, Mcintosh J R, Baumeister W (2005) 3D structure of eukaryotic flagella in a quiescent state revealed by cryo-electron tomography. *Proc. Natl Acad. Sci. U. S. A.* 102: 15889–15894.
35. Morone N, Nakada C, Umemura Y, Usukura J, Kusumi A (2008) Three-dimensional molecular architecture of the plasma-membrane-associated cytoskeleton as reconstructed by freeze-etch electron tomography. *Methods Cell Biol.* 88: 207–236.
36. Heuser J E, Anderson R G (1989) Hypertonic media inhibit receptor-mediated endocytosis by blocking clathrin-coated pit formation. *J. Cell Biol.* 108: 389–400.
37. Watanabe S, Punge A, Hollopeter G, Willig K I, Hobson R J, Davis M W, Hell S W, Jorgensen E M (2011) Protein localization in electron micrographs using fluorescence nanoscopy. *Nat. Methods* 8: 80–84.
38. Van Rijnsoever C, Oorschot V, Klumperman J (2008) Correlative light-electron microscopy (CLEM) combining live-cell imaging and immunolabeling of ultrathin cryosections. *Nat. Methods* 5: 973–980.
39. Grabenbauer M (2012) Correlative light and electron microscopy of GFP. *Methods Cell Biol.* 111: 117–138.